Yield determination of OH($v=0,1$) radicals produced by the electron-ion recombination of H_3O^+ ions

Theodosia Gougousi and Rainer Johnsen
Department of Physics and Astronomy, University of Pittsburgh, Pittsburgh, Pennsylvania 15260

Michael F. Golde
Department of Chemistry, University of Pittsburgh, Pittsburgh, Pennsylvania 15260

(Received 12 November 1996; accepted 13 May 1997)

A flowing afterglow apparatus in conjunction with laser induced fluorescence (LIF) diagnostics has been used to determine the yield of OH($v=0,1$) produced by the dissociative recombination (DR) of H_3O^+ ions with electrons at 300 K. The yield for $v=0$ radicals (0.48 ± 0.07) was determined by two different methods: (1) by comparing it to the known OH yield of the ion-molecule reaction $Ar^+ + H_2O$ and (2) by comparing it to that of the reaction of metastable Ar atoms (Ar*) with H_2O. The yield of vibrationally excited OH($v=1$) (0.12 ± 0.02) was obtained relative to that in $v=0$ by comparing LIF spectra. The results corroborate earlier experimental work which determined the yields of OH in $v=0$ and in unspecified vibrationally excited states $v>0$. © *1997 American Institute of Physics.* [S0021-9606(97)04131-7]

I. INTRODUCTION

Electron-ion dissociative recombination (DR)

$$e + AB^+ \rightarrow A + B \tag{1}$$

is often the dominant de-ionization process in cold, weakly ionized plasmas. Studies of the neutral reaction products are important for models of the chemical evolution of such media and they shed some light on the basic mechanism of dissociative recombination. Examples of ionized media where DR plays an important role are the terrestrial and planetary ionospheres,[1] interstellar gas clouds,[2,3] and industrial plasmas such as laser plasmas,[4] combustion flames[5] and processing plasmas used for etching[6] and deposition on semiconductor chips. If the gas phase chemistry of such media is to be understood, information is needed on both the recombination rate coefficients and product yields.

Total recombination coefficients α, and their variation with temperature, have been determined for a number of ions[7] using techniques such as stationary afterglows,[8–11] merged beams,[12–14] flowing afterglows,[15–17] and recently ion storage rings.[18,19] However, obtaining quantitative information on neutral products[20,21] of DR is experimentally far more difficult, and although considerable progress has been made in the last few years there still is a paucity of reliable data. Flowing afterglows have been the major source of data. Electronically excited states of species such as OH from O_2H^+ and N_2OH^+ ions,[22] NH from N_2OH^+,[22] and N_2H^+ ions,[23] CO from HCO^+,[23] and CO_2^+ ions,[24] and N_2 from N_2H^+ ions[23] have been identified using emission spectroscopy. Yields for the production of O atoms from the recombination of H_2O^+ (Ref. 25) and O_2^+ ions,[26] H atoms[27] from protonated species such as HCO^+, H_3O^+, CH_5^+, HCO_2^+, and OH radicals[28,29] from H_3O^+, HCO_2^+ and HN_2O^+ ions have also been determined. Merged-beam[30] and ion-storage-ring[31,19] experiments have provided H atom yields for H_3^+ ions and branching fractions for the recombination of H_3^+ and H_2D^+ ions.

Quantum-chemical calculations of product channels are quite difficult and have been carried out only for simple species such as HCO^+,[32] O_2^+,[33] and H_3^+.[34] For more complicated ions, only semi-quantitative propensity rules have been proposed. For instance, Green, Galloway and Herbst[35–37] have used a statistical phase space model to predict the products of DR for a number of ions whereas Bates[38–40] has used a more intuitive approach, arguing that the neutral products that involve the minimum rearrangement of atoms in the intermediate complex will be favored. The agreement between the existing theoretical predictions and experimental results is not generally very good and it is widely recognized that more experimental data are needed to guide the theory. In this paper, we will present measurements of the OH yield from H_3O^+ recombination. Results for other protonated ions have been obtained also and will be published in the accompanying paper.

Our flowing afterglow technique,[41] the use of Langmuir probes to measure electron densities,[42] and product detection by Laser Induced Fluorescence (LIF) share many features with earlier work,[15,28] but we have added spatially resolved LIF and rather extensive computer modeling of the afterglow processes. These improvements enable us to separate recombination products from those arising from extraneous sources. While similar information can be obtained if observations are carried out at a fixed location, position-sensitive detection of reaction products imposes a tighter constraint on the reaction models that are used in the analysis. For instance, it contains information on the loss of product particles to the walls, which otherwise has to be estimated. To test our methods, determination of OH($v=0$) and OH($v=1$) yields from the recombination of H_3O^+ provides a good system for study, since Herd *et al.*[29] measured a large OH yield

 0021-9606/97/107(7)/2430/10/$10.00

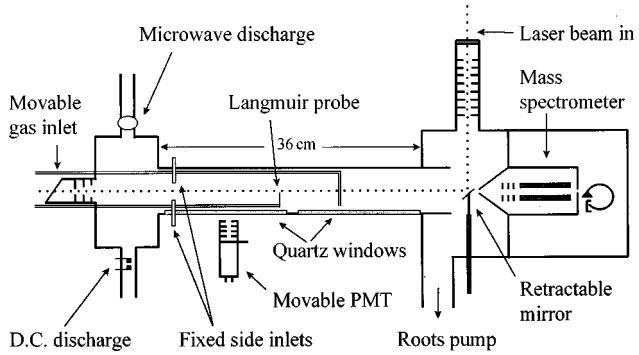

FIG. 1. Schematic diagram of the apparatus. For clarity, reagent inlets and the Langmuir probe have been rotated into the plane of the drawing. The central section of the flow tube has an internal diameter of 6 cm and a length of 36 cm. Spectroscopic and LIF observations are made through two quartz windows of length 15 cm each.

of 0.65 arising from two of the four exoergic channels[43]

$$H_3O^+ + e \rightarrow H_2O + H + 6.395\ \text{eV} \quad (2a)$$

$$\rightarrow OH + H_2 + 5.753\ \text{eV} \quad (2b)$$

$$\rightarrow OH + H + H + 1.275\ \text{eV} \quad (2c)$$

$$\rightarrow O + H_2 + H + 1.363\ \text{eV}. \quad (2d)$$

We note in passing that Bates[38] has argued that channel (2a) should be strongly favored over the other three because it involves the removal of only one valence-bound hydrogen atom. The experimental data do not seem to support this expectation.

II. EXPERIMENTAL METHODS

A. Flow tube apparatus

The flowing-afterglow technique[28] is well established and details of our flow tube[41] have also been described previously. The flow tube proper (a stainless steel tube of diameter 6 cm and length 36 cm) is shown in Fig. 1. A microwave discharge in He carrier gas produces mainly helium metastable atoms, $He^*(2^3S)$, which subsequently react with Ar added through the opposite inlet to produce Ar^+ ions via Penning ionization. The metastable helium atoms are destroyed in that process and none survive into the recombination region. The D.C. discharge shown in Fig. 1 is used only for certain calibration experiments as will be discussed in Section IV B; the two discharges are not operated at the same time. A quadrupole mass spectrometer at the downstream end of the tube is used to determine the ion composition of the plasma. Two long spectroscopic windows placed along the length permit spatially resolved observations. A movable Langmuir probe is used to monitor the electron density n_e on the tube axis as a function of distance z. Analysis of the electron density decay curves[41,44] provides a value for the recombination coefficient of the ion that dominates the plasma.

Under typical experimental conditions the electron densities in the upstream part of the tube are of the order of 5×10^{10} cm^{-3}, the flow tube pressure is 0.9 Torr and the flow is laminar with central velocity of ~5500 cm/s. Reagent gases are added mainly through a movable ''horseshoe'' inlet (diameter 3 cm) positioned 10–15 cm downstream of the Ar inlet and occasionally through four interconnected fixed finger inlets which are symmetrically positioned on a plane perpendicular to the tube axis in the upstream part of the tube (~10 cm from the Ar entry port).

B. Ion chemistry

The ion chemical steps in the production of the H_3O^+ ions are as follows: The microwave discharge in helium buffer gas produces primarily He* metastable atoms. Addition of argon (at about 20% of the helium pressure) downstream converts He* into Ar^+ ions and electrons via Penning ionization,

$$He^* + Ar \rightarrow He + Ar^+ + e, \quad (3)$$

thus creating an essentially non-recombining atomic-ion plasma. Addition of either pure H_2O or, alternatively, a mixture of H_2O and H_2 converts the Ar^+ ions into H_3O^+ ions. When pure H_2O is added (at a concentration of $[H_2O] \sim 10^{13}$ cm^{-3}), the product ions of the reaction[45]

$$Ar^+ + H_2O \rightarrow H_2O^+ + Ar \quad 68\% \quad (4a)$$

$$\rightarrow ArH^+ + OH \quad 32\% \quad (4b)$$

(overall rate constant: 1.2×10^{-9} cm^3 s^{-1}) rapidly convert into the desired H_3O^+ terminal ions,

$$H_2O^+ + H_2O \rightarrow H_3O^+ + OH, \quad k = 1.7 \times 10^{-9}\ \text{cm}^3\,\text{s}^{-1}, \quad (5)$$

$$ArH^+ + H_2O \rightarrow H_3O^+ + Ar, \quad k = 2.0 \times 10^{-9}\ \text{cm}^3\,\text{s}^{-1}. \quad (6)$$

Note that in this case OH radicals are produced at two places, in reactions (4b) and (5). At the high H_2O concentration used, almost all Ar^+ ions are converted to H_3O^+; one OH is produced, irrespective of the route, and the precise branching fraction in reaction (4) has little effect on the results presented here. If, however, a large concentration of H_2 is added along with the water vapor (typically $[H_2] \sim 10^{14}$ cm^{-3}, $[H_2O] \sim 10^{12}$ cm^{-3}) then the Ar^+ ions are preferentially converted to H_3^+ ions in the reactions

$$Ar^+ + H_2 \rightarrow ArH^+ + H, \quad k = 8 \times 10^{-10}\ \text{cm}^3\,\text{s}^{-1}, \quad (7)$$

$$ArH^+ + H_2 \rightarrow H_3^+ + Ar, \quad k = 9 \times 10^{-10}\ \text{cm}^3\,\text{s}^{-1}, \quad (8)$$

which subsequently transfer a proton to H_2O

$$H_3^+ + H_2O \rightarrow H_3O^+ + H_2, \quad k = 4.3 \times 10^{-9}\ \text{cm}^3\,\text{s}^{-1} \quad (9)$$

to produce H_3O^+. In this case the OH production from the ion-molecule reaction is reduced, but for higher H_2O concentrations ($[H_2O] \sim 10^{13}$ cm^{-3}) reactions (4b) and (5) are not entirely eliminated and should be included in a complete model.

If one wishes to determine the OH production from the *recombination* of the molecular ions with electrons,

$$H_3O^+ + e \rightarrow OH(v), \quad (10a)$$

$$H_3O^+ + e \rightarrow \text{other products}, \quad (10b)$$

and

$$H_2O^+ + e \rightarrow OH(v), \tag{11a}$$

$$H_2O^+ + e \rightarrow \text{other products}, \tag{11b}$$

the contribution arising from ion-molecule reactions (4b) and (5) must be separated. Our experimental method of distinguishing the two sources consisted of adding an electronegative gas (SF_6) that attaches free electrons rapidly[46–48] and thus eliminates electron-ion recombination. For SF_6 with an electron attachment coefficient of 3.1×10^{-7} cm^3/s at 300 K, addition of a very small amount ($[SF_6]\sim5\times10^{11}$ cm^{-3}) in the afterglow suffices to produce the desired effect. Because the reaction of SF_6 with Ar^+ ions is fairly fast ($k=1.2\times10^{-9}$ cm^3/s),[49]

$$Ar^+ + SF_6 \rightarrow SF_5^+ + F + Ar \tag{12}$$

addition of too much SF_6 has the undesired side-effect of changing the ion chemistry and producing free F atoms which could potentially disturb the neutral chemistry of the system. For that reason, the diagnostic tests with SF_6 were carried out using only minute traces of SF_6 added together with the reagent gases.

Another complication can arise from reactions of metastable Ar atoms, Ar*, which are also produced in the afterglow at about 10–15% of the Ar^+ ions. Their presence was traced by the appearance of N_2(C-B) emission[50] when N_2 was added in the afterglow and their concentration was determined from the measured ion yield from their reaction with NO.[51] The reaction of the metastables with H_2O leads to the production of both electronically excited and ground state OH (total yield 0.54)[52]

$$Ar^* + H_2O \rightarrow OH(X^2\Pi, v) + H + Ar \tag{13a}$$

$$\rightarrow OH(A^2\Sigma^+, v) + H + Ar \tag{13b}$$

which may be a significant source of radicals when only H_2O reagent is used. When H_2O/H_2 reagents are used most of the Ar* will react with the H_2 to produce H atoms, potentially complicating H atom measurements, and OH production from the reaction of the metastables with H_2O would be a minor channel.

In addition to ground-state OH, electronically excited OH can also be produced by the recombination reactions (10b) and (11b) and by reaction (13b). Indeed, OH(A→X) emissions were observed when either H_2O or H_2O/H_2 reagents were added to the afterglow. Although recombination of H_3O^+ ions releases sufficient energy to produce electronically excited OH [Eq. (2b)] our studies[53] have proved this a very small channel. Instead, we have found that the main source of these emissions are the recombination of H_2O^+ ions and the reaction of Ar* with H_2O. These emissions constitute a constant background for the LIF measurements which has to be considered when data are analyzed.

C. LIF detection of OH and data acquisition

The density of OH($v=0$) radicals in the afterglow is determined by exciting the $X^2\Pi$ ($v=0$)→ $A^2\Sigma^+$ ($v=0$) transition of OH with UV laser light and observing the fluorescence in the same transition. As shown in Fig. 1, the UV laser beam, generated by doubling the frequency of a pulsed excimer-pumped dye laser, enters the flow tube downstream in a direction perpendicular to the axis of the tube. An internal mirror, located in front of the mass spectrometer, deflects the laser beam on or very close to the tube axis towards the upstream direction. The beam exits from the tube through a well-baffled window. Multiple black baffles surround the laser entry and exit ports to minimize the scattered light. The mirror can be retracted from the tube, but it was found that it did not interfere with the operation of the mass spectrometer and it was usually left in place.

The repetition rate for the laser varied between 5 and 20 Hz and the dye laser output power was monitored by diverting a small fraction of the laser beam to a photodiode connected to an analog meter. The usual dye laser output energy was 0.1–0.5 mJ/pulse and care was taken that it did not vary by more than 5% throughout each experiment.

In most experiments, except for those described in Sec. IV C, the OH LIF signal was monitored by tuning the laser to the same transition, namely the $Q_1(3)$ peak. Using the same line for all LIF observations has the advantage that a higher laser intensity can be used, ensuring a reasonable LIF signal, and that transition saturation affects all measurements, including the calibration, by the same amount. Also, the laser tuning is facilitated and the operation is more stable at high intensities since the spectral lines are broadened due to the saturation effect.

A movable (in z-direction) photo-tube detects photons emanating from a small rectangular region (3 to 4 mm long) near the flow tube axis by means of an optical system that consists of a quartz lens (focal length 3.8 cm), a baffle and an interference filter (peak transmittance 0.22 at 310 nm, FWHM 15 nm). After amplification and pulse-height discrimination, the photomultiplier pulses are transferred to time-gated counters.

Background signals due to scattered laser light, electromagnetic interference and OH emissions from the reactions were subtracted. The remaining signal reflects OH arising from four different chemical sources, namely: (a) recombination of H_3O^+ ions [Eqs. (2b) and (2c)], (b) the ion-molecule reactions [Eqs. (4b) and (5)], (c) the recombination of the H_2O^+ intermediate ions [Eq. (11a), the OH yield has been measured[25] to be 0.55], and (d) the reaction of metastable Ar* atoms with H_2O [Eq. (13), the total OH yield has been measured[52] to be 0.54].

The relative OH contributions from sources (a) through (d) were separated by addition of the H_2 reagent to reduce sources (b) through (d), and by adding SF_6 to eliminate the recombination contribution. In addition, a high water concentration ($[H_2O]\sim10^{13}$ cm^{-3}) was maintained to reduce source (c). The OH LIF signal was recorded as a function of z for differing reagent combinations, repeating each measurement at least once to ensure reproducibility. Useful preliminary estimates of OH yields can be obtained by inspection of the raw data, but an accurate analysis requires

comparisons of the data to model calculations. Examples of such data are presented in Sec. IV.

Typical contributions from the extraneous sources (per 100 laser shots) were of the order of: 5–10 counts for scattered light, 5 counts for OH produced in the discharge and 0–2 counts for electrical pick-up while for the Ar* + H_2O reaction a contribution of 30 counts was calculated.

D. Reagent preparation and purity

Since it was found difficult to measure and to control the flow rate of H_2O a mixture of H_2O in He ($\sim$2.5% mole in H_2O) was prepared and the flow rate was calculated from the rate of pressure drop in a storage flask of known volume. The H_2O concentration in the flow tube was derived from the known flow conditions, pressure, mixture composition and temperature.

High-purity gases (He 99.997%, Ar 99.998%, H_2 99.999%) were used without further purification except for the use of cold traps in the gas handling system. The nitric oxide used in Sec. IV B, supplied by Matheson with a stated purity of 99%, was further purified by passing it through a soda lime trap at dry ice temperature, and by trap-to-trap distillation. Mass analysis showed that the distilled NO had a purity better than 99.5%. The NO used in section IV C was purified by passing it only through the soda lime trap. Even in this case no serious impurities were detected by the mass spectrometer. The H_2O used for the H_2O/He mixtures was subjected to several freeze, pump, thaw cycles before use.

III. COMPUTER MODELING OF THE AFTERGLOW

An afterglow is a rather complicated system in which the various species diffuse and participate in the chemistry while flowing along the tube. If absolute product yields are to be determined the LIF measurements have to be correlated with the absolute number densities of the relevant product, not a straightforward process because of the complexity of the system.

For example, in the afterglow the charge is transferred from the Ar^+ ions to intermediate ions until the desired terminal ion is produced, and three different diffusion regions can be identified: Upstream of the reagent inlet an Ar^+/e non-recombining plasma exists. In the region around the reagent inlet (gas mixing region) several different ions coexist for 1–2 cm and a transition occurs from diffusion to recombination dominated plasma. Finally, the desired terminal ion is produced and its recombination dominates the plasma. Furthermore, recombination creates large gradients in the electron density in the axial direction which have to be included in the diffusive description of the system. For all these reasons a simple description of the plasma processes is not possible and the only way of understanding its ''behavior'' is by modeling it.

The continuity equation in a parabolic flow profile for each species i present in the afterglow is of the form:

$$\frac{dn_i(r,z)}{dt} = \text{chemistry terms} + D\left(\frac{\partial^2 n_i}{\partial z^2} + \frac{1}{r}\frac{\partial}{\partial r}\left(r\frac{\partial n_i}{\partial r}\right)\right) - v_0\left(1-\frac{r^2}{R^2}\right)\frac{\partial n_i}{\partial z}, \tag{14}$$

where $n_i(r,z)$ is the species number density as a function of position along the flow tube, D is the ambipolar diffusion coefficient for ionic species or the diffusion coefficient for neutral species, v_0 is the central velocity and R the flow tube radius. The equation has three terms: The ''chemistry'' term represents all ion-molecule and electron-ion recombination reactions in which a specific species participates. The ''diffusion'' describes axial and radial diffusion of the species in cylindrical geometry. Finally, the last term describes the gas flow which has a parabolic velocity profile. The equation is applicable to both uncharged and charged species if one imposes the constraint that the density of charged particles tends to zero at the walls and that the plasma is electrically neutral.

Since this equation cannot be solved analytically we had to use numerical methods. An explicit method might be the obvious choice but its poor convergence properties are a major drawback. For that reason a mixed explicit-implicit method [alternating-direction implicit (ADI)][54] was used, and the equation was solved as a function of time until steady state was reached which is the situation in the flow tube. The basic idea of that method is to divide each time step Δt into two steps of size $\Delta t/2$ and in each substep treat implicitly a different dimension (axial–radial). The radial and axial steps were both chosen 0.1 cm, thus creating a grid of 200 steps (20 cm) in the axial direction and 30 steps (3 cm) in the radial direction, and the time step was 10^{-5} s. The stability of the algorithm was checked by varying both the space and time steps until we were convinced that with the above stated values convergence occurred to the correct steady-state values.

The equation could be applied in two ways, either for the spatial distribution of a single species, using known concentrations of all other relevant species; or simultaneously for several reactive species. The latter mode was used in the present system to analyze the plasma containing ArH^+, H_3^+, H_3O^+ and electrons; then the former mode was used to simulate OH production from the channels discussed above. The yield of OH production from H_3O^+ recombination was determined by comparison of the calculated OH concentrations and the measured OH signals.

In a realistic model many parameters have to be included. Ambipolar diffusion coefficients for all the ions are calculated from the measured mobilities[55–57] in helium and argon using Einstein's relation between diffusion and mobility. In cases where the mobilities in argon are not known the Langevin formula[58] is used to obtain an estimate.

The recombination coefficients α for H_3O^+, H_2O^+ and H_3^+ enter critically into the model. A value of $\alpha(H_3O^+)=8.0\times10^{-7}$ cm^3/s was determined in this experiment,[44] in good agreement with previously reported values.[59,29] Because of the complicated reaction scheme a

value for the H_2O^+ recombination coefficient could not be obtained. However, a previous measurement[60] gave a value of 3.2×10^{-7} cm^3/s and this was used in the models.

There is an ongoing controversy regarding the recombination coefficient for H_3^+ ions.[61,62,41] It has been previously observed that the decay of a H_3^+/e plasma is anomalous[62,41] in the sense that it does not obey a simple binary recombination law. It recombines quite efficiently at high electron densities (for $n_e\sim5\times10^{10}$ cm^{-3}, effective $\alpha\sim2\times10^{-7}$ cm^3/s) but less rapidly as the electron density decays (for $n_e\sim10^9$ cm^{-3}, effective $\alpha\sim10^{-8}$ cm^3/s). In our experiments, the amounts of H_2 and H_2O added are such that the Ar^+ ions are initially converted into H_3^+ ions, which subsequently transfer a proton to H_2O to produce the H_3O^+ terminal ions. The H_3^+ ions are formed in a region of high electron densities and a value of 2×10^{-7} cm^3/s for the effective recombination coefficient which we measured under similar experimental conditions is appropriate.

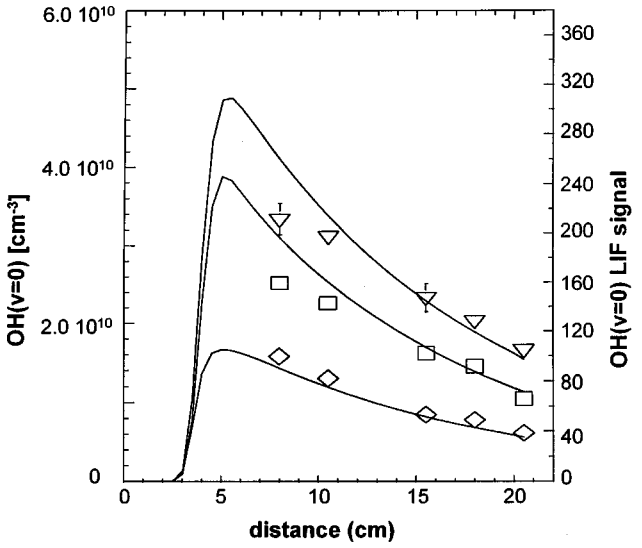

FIG. 2. OH($v=0$) LIF data (fluorescence photon counts per 50 laser shots) obtained for H_2O (triangles), H_2O/SF_6 (squares) and H_2O/H_2 (diamonds) reagent gases. The solid lines are model generated OH distributions (using a yield of 0.48 for the OH($v=0$) production from the recombination of H_3O^+ ions) and the three data sets have been normalized to the model predictions by a common factor.

IV. RESULTS

A portion of the OH($v=0$ $X^2\Pi\rightarrow$ $v=0$ $A^2\Sigma^+$) excitation spectrum was obtained by scanning the laser wavelength from 307.8 to 309.0 nm. Examination of the relative intensities of the lines showed that the rotational level population distribution of OH($X^2\Pi$, $v=0$) obeyed a Boltzmann distribution at 290 ± 40 K, which means that the rotational mode of the OH product is thermalized to the gas temperature before laser excitation. However, collisional thermalization of the vibrational mode is much slower,[63] so that the nascent vibrational distribution persists long enough to be observable, and as will be discussed later, absolute yields for OH($X^2\Pi$) in the $v=0$ and $v=1$ levels were measured.

A. Yield determination of OH($v=0$) from H_3O^+ recombination using the ion-molecule reactions as a reference source of OH

Addition of varying concentrations of H_2O, H_2O/H_2 or H_2O/SF_6 alters the relative OH contributions from different sources, as is clearly demonstrated by the data sample in Fig. 2. No LIF observation could be made close to the H_2O reagent inlet because the OH($A\rightarrow X$) emissions masked the LIF signal. From such data, the OH($v=0$) yield f from H_3O^+ recombination was obtained by adjusting its value in the computer model until the model predictions best reproduced the data. The rapid wall loss in the OH signal well downstream from the reaction zone (see Fig. 2) is consistent with wall removal of OH with unit efficiency. All the other parameters used in the model simulations are known from the literature, as discussed earlier. The uncertainties in those parameters would have insignificant effects on the derived OH yield. In this method of fitting the data, the OH yield of the ion-molecule reactions (4b) and (5) provides a known source of OH, which permits the absolute yield determination. The assumption is made that the ion-molecule reaction (4b) produces exclusively OH($v=0$). It is not certain that this assumption is valid and this was one reason why a second, independent method of calibrating the OH LIF signal was used (see Sec. IV B). Based on three different experiments and a total of 40 points a value of

$$f=0.51\pm0.09$$

was obtained for the OH($v=0$) production from the recombination of H_3O^+ ions, the uncertainty being the standard deviation of the measurements from the mean value.

A sensitivity analysis was undertaken to see how strongly the assumed value for the yield of OH($v=0$) from the recombination of H_2O^+ affected this result. The results showed that variation of this yield from 0 to 1 changed the best value of f by at most 2%, which is not surprising, since under our experimental conditions most H_2O^+ ions react further rather than recombine.

B. Yield of OH($v=0$) from H_3O^+ recombination using the reaction of Ar* with H_2O as a reference source of OH

The reactions of metastable argon atoms, Ar*, with NO and H_2O

$$Ar^*+NO\rightarrow NO^++e+Ar \text{ (yield } 0.28\pm0.10\text{) (Ref. 51),} \quad (15)$$

$$Ar^*+H_2O\rightarrow OH+H+Ar \text{ (total OH yield } 0.54\pm0.04\text{) (Ref. 52),} \quad (16)$$

were used as an alternative way of calibrating the LIF optical detection system. The known yield in reaction 16 refers to the total production of OH. Using the technique described in Sec. IV C we were able to determine that OH($v=0$) has a 0.48 ± 0.10 production yield in reaction 16, and this value was used in the data analysis.

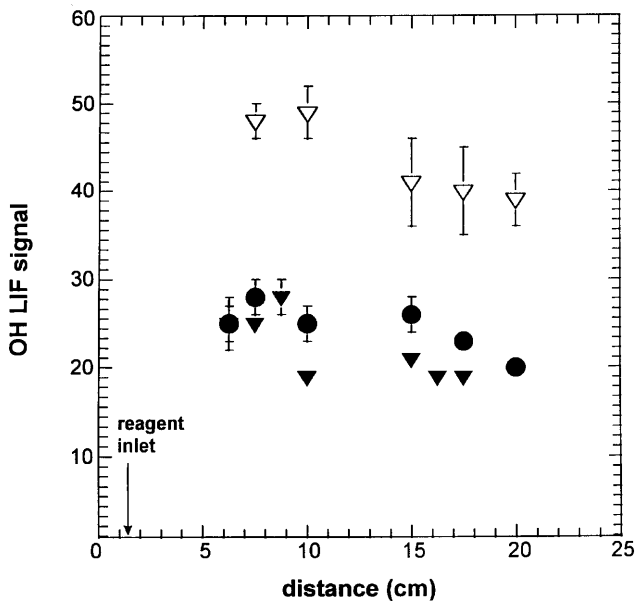

FIG. 3. OH($v=0$) LIF data obtained for the reaction of Ar* with H_2O. Three different data sets are shown. In comparison with Fig. 2 the decay of the OH LIF signal is much slower.

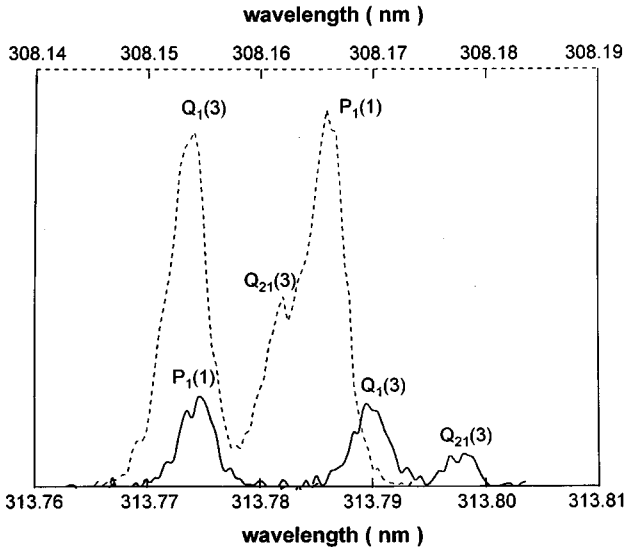

FIG. 4. Laser excitation spectra of OH($v=0$) (dashed line) and OH($v=1$) (solid line) produced by the dissociative recombination of H_3O^+ ions with electrons. The top (dashed) axis refers to the OH($v=0$) spectrum and the bottom (solid) axis to the OH($v=1$). Both spectra have been corrected for background. In the OH($v=1$) spectrum the intensity ratio of the $Q_{21}(3)$ to the $Q_1(3)$ line is ~0.4 whereas the theoretical prediction is 0.21, indicating that the transition has been partially saturated.

For these experiments Ar metastable atoms were produced in a D.C. discharge running in argon buffer gas (0.67 Torr), and helium (0.43 Torr) was added to increase the pressure in the flow tube. The number of Ar* produced was found to depend critically on both the Ar and the total pressure in the flow tube. H_2O was added through the reagent inlet and the OH($v=0$) LIF signal was recorded as a function of position. In order to measure the absolute concentration of Ar*, the H_2O was replaced by NO , thus converting Ar* to NO^+ ions and electrons, and the electron density was measured with the Langmuir probe. Since the electron density produced by the Ar*+NO reaction was $1–2\times10^9$ cm^{-3}, it was unnecessary to correct for the recombination loss of NO^+ ions.

Then, the normal buffer gas flow rates were reestablished and the microwave discharge scheme was used to produce H_3O^+ ions with the addition of H_2/H_2O reagents as described earlier. The OH($v=0$) LIF signal was recorded as a function of position and the model was used to calculate OH contributions as described in Sec. III. Comparison between the LIF data, the model predictions and the calibration factor derived above, provided the desired yield. Three different experiments with a total of 15 points produced a yield of

$$f=0.44\pm0.11$$

the uncertainty including the propagated errors from all sources. Sample data for the OH($X^2\Pi$, $v=0$) LIF signal from the Ar*+H_2O reaction are presented in Fig. 3. The data shown in the figure clearly indicate that the wall loss of OH was smaller under these conditions than those in Fig. 2. As will be discussed further in Sec. V, the rate at which OH is lost at the walls seems to depend on some poorly controlled factors. It is one advantage of position-sensitive LIF measurements that this quantity can be measured directly.

C. OH($v=1$) yield from H_3O^+ recombination

The yield of OH($v=1$) can be determined relative to that of OH($v=0$) (yield 0.48 ± 0.07) by comparing OH LIF spectra recorded for the same lines of the (0,0) and (1,1) bands for the OH($X^2\Pi\rightarrow A^2\Sigma^+$) transition (see Fig. 4). Analysis of the spectra involved comparison of both the peak heights and the peak areas for the $Q_1(3)$ line in both bands (308.16 nm for the (0,0) transition and 313.78 nm for the (1,1) transition). In order to convert the ratio of signal intensities into a ratio of vibrational populations, corrections for differences in rotational line strengths, and Franck-Condon factors of the transition were required. In addition, the effects of partial saturation of the transition and the transmittance of the 310 nm narrow-band filter were considered.

Partial saturation of the transition at the relative high laser pulse energies used is the major problem of such type of analysis. In order to examine the saturation effects the $Q_{21}(3)$ and $Q_1(3)$ lines were chosen and spectra were recorded for laser pulse energies different by as much as a factor of four, as can be seen in Fig. 5. These lines originate from the same lower level and comparison of the theoretical to experimentally determined intensities can provide us with an estimate of the degree of the transition saturation. The expected ratio of the $Q_{21}(3)$ intensity to that of $Q_1(3)$ is 0.21 according to Dieke and Crosswhite,[64] whereas the experimentally determined ratios were between 0.3 and 0.4, the laser pulse energies not having a big effect on the relative peak heights. For unsaturated transitions the peak height should vary linearly with the laser pulse energy. In our case

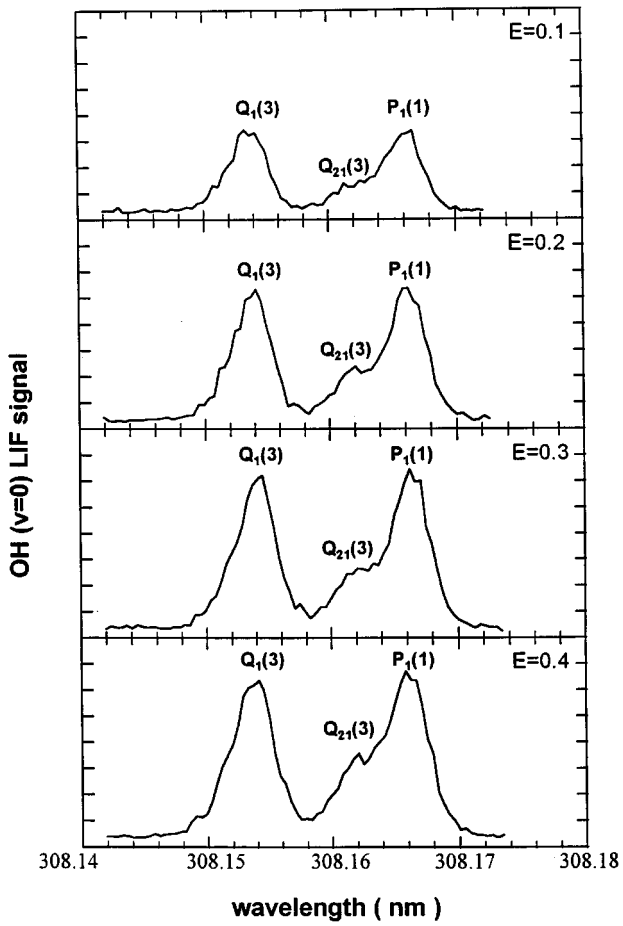

FIG. 5. LIF spectra of OH($v=0$) (fluorescence photon counts per 100 laser shots) produced by the dissociative recombination of H_3O^+ ions with electrons for different dye laser pulse energies E (E in arbitrary units). The spectra were obtained by scanning the laser wavelength through the $Q_1(K)$ lines of the OH($X^2\Pi \rightarrow A^2\Sigma^+$) transition.

we find that the dependence is that of laser pulse energy to the power 0.6 which indicates that the transition is only partially saturated. Lowering the laser power might result in the elimination of the saturation problems, but at the same time the signal for the (1,1) transition would become very small.

If there are no saturation problems the full correction for the different Franck-Condon factors (0.906 for the (0,0) and 0.708 for the (1,1) bands)[65] of the two transitions must be applied. If, on the other hand, the transition is completely saturated, then no correction should be applied. Since in our case we found that the exponent in the peak height vs. laser pulse energy plots is 0.6, the same correction for the different Franck-Condon factors was applied.

Another complication may arise from the difference in the filter transmission for the two spectral regions, 308 nm for the (0,0) and 314 nm for the (1,1) transition, used in the LIF spectra comparison. Excitation of the $Q_1(3)$ line was mainly used in those experiments. Rotational relaxation[66] of this state in collisions with Ar and He led to a population redistribution prior to de-excitation and the observed fluorescence signal originated from several branches through a range of wavelengths. Analysis that included the spectral response of the filter, and the de-excitation through the various branches led to the conclusion that we were discriminating against the OH($v=1$) by about 10%.

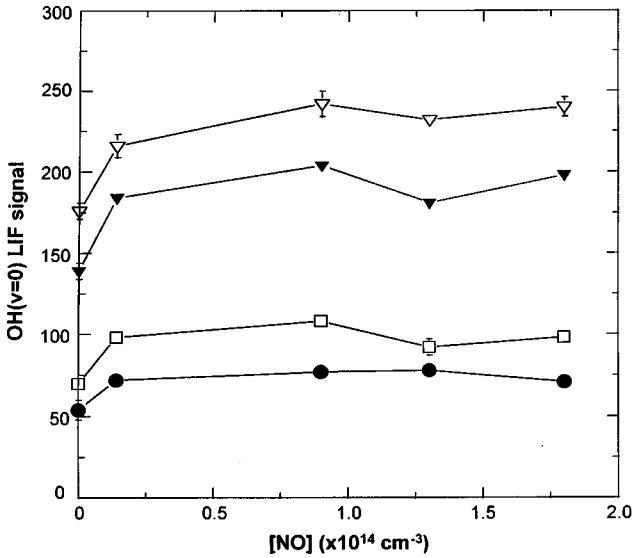

FIG. 6. Variation of the OH($v=0$) LIF signal (fluorescence photon counts per 100 laser shots) with the NO concentration added in the afterglow. The four data sets refer to observations at different distances from the reagent inlet (open triangles: 5 cm, filled triangles: 7 cm, open squares: 12 cm, filled circles: 15 cm).

Taking all these effects into account a yield of

$$f = 0.12 \pm 0.02$$

for the OH($v=1$) produced by the recombination of H_3O^+ ions was found, which is the average derived for six experiments, the uncertainty including the propagated errors from all sources involved.

An alternative way of determining yields for vibrationally excited OH has been used by Adams *et al.*[28] OH($v>0$) is known to vibrationally relax in collisions with NO. Thus, addition of NO downstream of the main reagent inlet but upstream of the LIF port should lead to an increase of the OH($v=0$) LIF signal which would be attributed to the quenching of OH($v \geq 1$) to the ground state. Once enough NO has been added, comparison of the LIF signal in the presence of NO to that when no NO is added, provides a yield for the production of OH($v \geq 1$). Following that suggestion we used the fixed side inlets (see Fig. 1) to add the reagent gases and the movable reagent inlet to add NO at a distance of about 6 cm downstream of the reagent gas addition port. Addition of NO indeed increased the OH($v=0$) signal (see Fig. 6) and comparison of the LIF signals, as described above, provided a yield of

$$f = 0.17 \pm 0.04$$

for the production of vibrationally excited OH.

V. DISCUSSION

The absolute yield of OH($v=0$) was determined by two *independent* methods and the agreement was excellent. The only previous measurement for H_3O^+ ions is that of Herd

TABLE I. Comparison between the results obtained in this work and those of Herd *et al.*

Yield	This work	Herd *et al.*
OH($v=0$)	0.48 ± 0.07	0.46 ± 0.07
OH($v=1$)	0.12 ± 0.02	-
OH($v\geqslant1$)	0.17 ± 0.04	0.19 ± 0.03

et al.,[29] also made in a flowing afterglow but without the use of computer modeling. As can be seen in Table I, the yields for OH($v=0$) are essentially the same, a most gratifying result in view of the differing experimental procedures.

Herd *et al.*[29] determined the yield for vibrationally excited OH($v\geqslant1$) by quenching those to the vibrational ground state. By using the same method, we derived a yield of

$$f=0.17\pm0.04$$

for vibrationally excited OH, again in good agreement with Herd *et al.*'s value of 0.19. Our specific yield of 0.12 for OH($v=1$) indicates that most of the vibrational excitation is concentrated in $v=1$. Perhaps the additional yield of 0.05 ± 0.04 should be ascribed to the production of OH($v\geqslant2$). Such a result is consistent with a Boltzmann distribution with a vibrational temperature of approximately 2000 ± 300 K.

In order to check the validity of both the model and the parameters used, the OH LIF signal produced by the recombination of H_3O^+ ions in an H_2/H_2O afterglow was recorded for a constant H_2 and three different H_2O concentrations. When a low H_2O concentration ($[H_2O]\sim5\times10^{11}$ cm^{-3}) is used the time for the completion of the proton transfer reaction is quite large. Efficient recombination ($\alpha\sim10^{-7}$ cm^3/s) for the H_3^+ ions would then ensure a significant loss of the precursor ion, resulting in low H_3O^+ and subsequently OH production. For high H_2O concentrations ($[H_2O]\sim5\times10^{12}$ cm^{-3}), the proton transfer would proceed much faster resulting in much larger H_3O^+ and OH production. If the H_3^+ ions do not recombine efficiently ($\alpha\sim10^{-8}$ cm^3/s) then no significant difference in the production of OH should be expected. The experimental data (Fig. 7) show a considerable difference in the OH signal between high and low H_2O concentrations indicating efficient removal of the H_3^+ ions because of recombination.

OH product distributions for the different conditions were determined by the model and were compared with the experimental data using a common weighting factor for all three data sets. As can be seen in Fig. 7 there is very good agreement between the model predictions and the LIF data, in (i) simulating the rise and the decay of the signal for each data set separately and (ii) predicting the difference in the OH concentrations for the different H_2O reagent concentrations. The excellent agreement between the model predictions and the LIF data indicate that the values used for the parameters and especially those for the recombination coefficients of H_3O^+ and H_3^+ ions are realistic. It must be noted here that the same simulation was run with the values for all the parameters constant except that for the recombination coefficient for H_3^+ ions which was set at 2×10^{-8} cm^3/s.

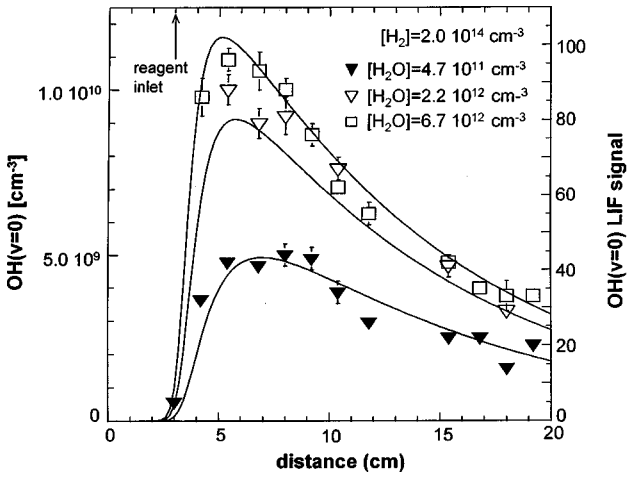

FIG. 7. OH($v=0$) LIF data (fluorescence photon counts per 50 laser shots) obtained for a steady H_2 concentration and three different H_2O concentrations. Noteworthy is the difference in the LIF signal for the high and the low H_2O concentrations. The solid lines are model generated OH distributions and the three data sets have been weighted to the model predictions by a common factor.

Under these conditions the considerable difference in the OH signal for the different reagent gas compositions could not be reproduced and a common weighting factor for all three data sets could not be found. We consider that an adequate proof that at least in high electron density afterglow plasmas ($n_e>10^{10}$ cm^{-3}), a value of 2×10^{-7} cm^3/s should be used for the recombination coefficient of H_3^+ ions.

The importance of using spatially resolved LIF and the detailed modeling is illustrated by the measured OH profiles. In the $Ar^+ + H_2O/H_2$ system (Fig. 2 and Fig. 7) the OH signal decayed rapidly downstream, consistent with efficient wall loss of this radical. In contrast, OH, generated via the $Ar^* + H_2O$ reaction, showed a much smaller wall loss, as shown in Fig. 3. We and others have observed a similar behavior previously.[67,68] Clearly, if measurements had been made at a single point far downstream, it would have been very difficult to detect, and therefore allow for this difference in wall loss efficiency.

This study and previous work provide the following information concerning the products of dissociative recombination of H_3O^+. OH($X^2\Pi$) is formed in the majority of recombination events, but with less than unit efficiency. The yield of electronically excited OH($A^2\Sigma^+$) is very small. The measured yield of H atoms[27] suggests that the channels leading to $OH+H_2$ and $OH+H+H$ are both important. It is anticipated that H_2O+H, rather than $O+H_2+H$, accounts for most of the remaining $\sim30\%$ of recombination. It is of interest to compare these findings with what is known about the structures of H_3O and H_3O^+.

H_3O^+ has C_{3v} symmetry with an H-H separation of ~0.130 nm.[69] The formation of $OH+H_2$, therefore, involves a very large change in this distance and is expected to be important only if the long-lived H_3O^* intermediate undergoes extensive vibrational motion. Thus, an appreciable yield of $OH+H_2$ would seem to provide evidence *against* a ''direct'' model for dissociative recombination, i.e. one domi-

nated by efficient crossing to a strongly-repulsive valence state of H_3O.

Ab initio calculations[69] appear to support this conclusion. Because of the very large proton affinity of water, the ground state of H_3O^+ lies only 6.2 eV above $H_2O(X)+H$ (^2S). At the equilibrium geometry of H_3O^+, the lowest two electronic states of H_3O, 1^2A_1 and 1^2E, have appreciable Rydberg character. The ground state is calculated to lie about 0.7 eV above H_2O+H, but to be weakly bound with a small barrier of about 0.16 eV. This implies that access to the $H_2O(X)+H$ products can only occur via ground state H_3O. $H_3O(1^2A_1)$ also correlates (via a change in symmetry) with $OH(X^2\Pi)+H_2$, via a larger barrier of ~ 1 eV (the transition state could not be precisely located).

$OH(X^2\Pi)+H_2$ also give rise to another surface (e.g. $^2A''$ in C_s symmetry). This must correlate with the first excited state of H_3O, but details of this region of the potential energy surface are not known. The calculations suggested a large H-H separation in the transition state, such that dissociation along this channel might yield $OH+H+H$.

At high energies, families of Rydberg states are expected, but very few valence states, only those correlating with $OH(A^2\Sigma^+)+H_2$ and H_2+H+O. These lie at such high energies that access from H_3O^++e may not occur readily: indeed, the yield of $OH(A^2\Sigma^+)$ is clearly very small.

Because of the non-crossing of states of common symmetry below the ionization limit, recombination is likely to lead initially to formation of high Rydberg states of H_3O. These may be relatively long-lived. Their decay can involve two distinct mechanisms. First, coupling with other Rydberg states can lead to population of lower-lying states but with the total internal energy of the molecule remaining constant. Thus, if low-lying states such as 1^2A_1 and 1^2E are populated, the molecules will acquire very large amounts of vibrational energy. Second, radiative or even collisional relaxation leads to population of lower states of H_3O, but with smaller extents of vibrational excitation.

This picture of the mechanism of dissociative recombination can explain the observation of several product channels for this reaction. The large yield of OH is consistent with extensive dissociation via the first excited state of H_3O. If it is confirmed that H_2O+H is the other major product, this would suggest that part of the recombination occurs via the ground state of H_3O. The small degree of vibrational excitation in OH is consistent with the fact that the O-H bond lengths of H_3O^+, $H_3O(X)$, H_2O and OH are all very similar. Thus, there is no need for large changes in R_{OH} to occur during the dissociation process. In contrast, vibrational excitation of any H_2 product and rotational excitation of both OH and H_2 are expected: unfortunately, neither can be studied with the present form of the apparatus.

It is clear that we have not yet reached a clear understanding of the mechanism of recombinations of polyatomic ions. For instance, the approach taken by Bates[70] to explain the vibrational excitation of recombination products provides an intuitively appealing picture, but it does not truly reproduce experimental data. In the case of H_3O^+ recombination, Bates' arguments predict that 18% of the OH radicals should be vibrationally excited, which is not too different from the experimental ratio of 29%. However, according to his model, only the even ($v=0,2,4,...$) vibrational levels should be excited, while our experiment shows that the $v=1$ level is favored.

VI. CONCLUSIONS

The flowing afterglow technique combined with computer modeling has been developed for the determination of absolute yields for the production of $OH(v=0,1)$ from the electron-ion dissociative recombination of H_3O^+ ions. Two independent methods have been used for the determination of $OH(v=0)$ yield and the results obtained are in excellent agreement. The yield for $OH(v=1)$ has been determined relative to that of $OH(v=0)$ by comparison of LIF spectra, with corrections applied for possible transition saturation effects. Excellent agreement has been found with the results obtained previously by Herd *et al.*[29] Spatially resolved LIF measurements combined with computer modeling of the afterglow were found to be both practical and useful tools for the derivation of absolute product yields.

After this article had been submitted for publication, two new measurements of product yields from H_3O^+ recombination have been published. Ion-storage-ring measurements by Anderson *et al.*[71] have now yielded complete branching fractions for all channels of reaction 2 and Williams *et al.*[72] report flowing-afterglow measurements of the same branching fractions. The ion storage ring data do not distinguish OH radicals in different vibrational states, but the total OH yield agrees precisely with the numbers reported by us and the results of the earlier work by Herd *et al*. This most gratifying convergence of results unfortunately does not yet extend to the O-atom channel (2d), since the two new measurements gave rather different results.

ACKNOWLEDGMENTS

This work was in part supported by NASA under Grant No. NAGW 1764. Theodosia Gougousi is grateful to the Andrew Mellon Foundation for providing a pre-doctoral fellowship.

[1] G. C. Reid, Adv. At. Mol. Phys. **63**, 375 (1976).
[2] A. Dalgarno and J. H. Black, Rep. Prog. Phys. **39**, 573 (1976).
[3] T. J. Millar, D. J. DeFrees, A. D. McLean, and E. Herbst, Astron. Astrophys. **194**, 250 (1988).
[4] J. B. Laudenslager, *Kinetics of Ion-Molecule Reactions* (Plenum, New York, 1979), p. 405.
[5] J. M. Goodings, N. S. Karellas, and C. S. Hassanali, Int. J. Mass Spectrom. Ion Proc. **89**, 205 (1989).
[6] G. Turban, Pure Appl. Chem. **56**, 215 (1984).
[7] J. B. A. Mitchell, Phys. Rep. **186**, 217 (1990).
[8] F. J. Mehr and M. A. Biondi, Phys. Rev. **181**, 264 (1969).
[9] C. S. Weller and M. A. Biondi, Phys. Rev. Lett. **19**, 59 (1967).
[10] C. M. Huang, M. A. Biondi, and R. Johnsen, Phys. Rev. A **11**, 901 (1975).
[11] R. Johnsen, Int. J. Mass Spectrom. Ion Process **81**, 67 (1987).
[12] D. Auerbach, R. Cacak, R. Caudano, T. D. Gaily, C. J. Keyser, J. Wm. McGowan, J. B. A. Mitchell, and S. F. J. Wilk, J. Phys. B **10**, 3797 (1977).
[13] P. M. Mul, J. Wm. McGowan, P. Defrance, and J. B. A. Mitchell, J. Phys. B **16**, 3099 (1983).

[14] F. B. Yousif, J. B. A. Mitchell, M. Rogelstad, A. Le Paddelec, A. Canosa, and M. I. Chibisov, Phys. Rev. A **49**, 4610 (1994).
[15] E. Alge, N. G. Adams, and D. Smith, J. Phys. B **16**, 1433 (1983).
[16] N. G. Adams and D. Smith, Chem. Phys. Lett. **144**, 11 (1988).
[17] A. Canosa, J. C. Gomet, B. R. Rowe, and J. L. Queffelec, J. Chem. Phys. **94**, 7159 (1991).
[18] M. Larsson, Int. J. Mass Spectrom. Ion Process **149/150**, 403 (1995).
[19] S. Datz, M. Larsson, C. Stromholm, G. Sundström, V. Zengin, H. Danared, A. Källberg, and M. af Ugglas, Phys. Rev. A **52**, 2901 (1995).
[20] B. R. Rowe and J. L. Queffelec, *Dissociative Recombination: Theory, Experiment and Application* (World Scientific, Singapore, 1989), p. 151.
[21] N. G. Adams, *Advances in Gas Phase Ion Chemistry* (JAI, Greenwich, 1992), Vol. 1, p. 271.
[22] B. L. Foley, N. G. Adams, and H. S. Lee, J. Phys. Chem. **97**, 5218 (1993).
[23] N. G. Adams and L. M. Babcock, J. Phys. Chem. **98**, 4564 (1994).
[24] M. Tsuji. M. Nakamura, and Y. Nishimura, J. Chem. Phys. **103**, 1413 (1995).
[25] B. R. Rowe, F. Vallee, J. L. Queffelec, J. C. Gomet, and M. Morlais, J. Chem. Phys. **88**, 845 (1988).
[26] J. L. Queffelec, B. R. Rowe, F. Vallee, J. C. Gomet, and M. Morlais, J. Chem. Phys. **91**, 5335 (1989).
[27] N. G. Adams, C. R. Herd, M. Geoghegan, D. Smith, A. Canosa, J. C. Gomet, B. R. Rowe, J. L. Queffelec, and M. Morlais, J. Chem. Phys. **94**, 4852 (1991).
[28] N. G. Adams, C. R. Herd, and D. Smith, J. Chem. Phys. **91**, 963 (1989).
[29] C. Herd, N. G. Adams, and D. Smith, Astrophys. J. **349**, 388 (1990).
[30] J. B. A. Mitchell, J. L. Forand, C. T. Ng, D. P. Levac, R. E. Mitchell, P. M. Mul, W. Clayes, A. Sen, and J. Wm. McGowan, Phys. Rev. Lett. **51**, 885 (1983).
[31] S. Datz, G. Sundström, C. Biedermann, L. Broström, H. Danared, S. Mannervik, J. R. Mowat, and M. Larsson, Phys. Rev. Lett. **74**, 896 (1995).
[32] W. P. Kraemer and A. U. Hazi, *Dissociative Recombination: Theory, Experiment and Application* (World Scientific, Singapore, 1989), p. 61.
[33] S. L. Guberman, *Physics of Ion-Ion and Electron-Ion Collisions* (Plenum, New York, 1983), p. 167.
[34] H. H. Michels and R. H. Hobbs, Astrophys. J. **286**, L27 (1984).
[35] S. Green and E. Herbst, Astrophys. J. **229**, 121 (1979).
[36] E. Herbst, Appl. J. **222**, 508 (1978).
[37] E. T. Galloway and E. Herbst, Astrophys. J. **376**, 531 (1991).
[38] D. R. Bates, Astrophys. J. **306**, L45 (1986).
[39] D. R. Bates, J. Phys. B **24**, 3267(1991).
[40] D. R. Bates, Astrophys. J. **344**, 531 (1989).
[41] T. Gougousi, R. Johnsen, and M. F. Golde, Int. J. Mass Spectrom. Ion Process **149/150**, 131 (1995).
[42] R. Johnsen, E. V. Shun'ko, T. Gougousi, and M. F. Golde, Phys. Rev. E **50**, 3994 (1994).
[43] A. A. Radzig and B. M. Smirnov, *Reference Data on Atoms, Molecules and Ions* (Springer, Berlin, 1980).
[44] T. Gougousi, M. F. Golde, and R. Johnsen, Chem. Phys. Lett. **265**, 399 (1997).
[45] C. J. Howard, H. W. Rundle, and F. Kaufman, J. Chem. Phys. **53**, 3745 (1970).
[46] J. Balamuta, M. F. Golde, and Y. S. Ho, J. Chem. Phys. **79**, 2822 (1983).
[47] L. A. Gundel, D. W. Setser, M. A. A. Clyne, J. A. Coxon, and W. Nip, J. Chem. Phys. **64**, 4390 (1976).
[48] D. Smith, N. G. Adams, and E. Alge, J. Phys. B **17**, 461 (1984).
[49] D. L. Albritton, At. Data Nucl. Tables **22**, 1 (1978).
[50] J. H. Kolts, H. C. Brashears, and D. W. Setser, J. Chem. Phys. **67**, 2931 (1977).
[51] M. F. Golde, Y. S. Ho, and H. Ogura, J. Chem. Phys. **76**, 3535 (1982).
[52] J. Balamuta and M. F. Golde, J. Chem. Phys. **76**, 2430 (1982).
[53] T. Gougousi, M. F. Golde, and R. Johnsen (unpublished).
[54] W. H. Press, W. Vetterling, S. A. Teukolsky, and B. Flannery, *Numerical Recipes in Fortran*, 2nd ed. (Cambridge University Press, Cambridge, 1992), pp. 847, 861.
[55] H. W. Ellis, R. Y. Pai, E. W. McDaniel, E. A. Mason, and L. A. Viehland, At. Data Nucl. Tables **17**, 177 (1976).
[56] H. W. Ellis, E. W. McDaniel, D. L. Albritton, L. A. Viehland, S. L. Lin, and E. A. Mason, At. Data Nucl. Tables **22**, 179 (1978).
[57] H. W. Ellis, M. G. Thackston, E. W. McDaniel, and E. A. Mason, At. Data Nucl. Tables **31**, 113 (1984).
[58] E. W. McDaniel, J. B. A. Mitchell, and M. E. Rudd, *Atomic Collisions: Heavy Particle Projectiles* (Wiley, New York, 1993), p. 498.
[59] M. T. Leu, M. A. Biondi, and R. Johnsen, Phys. Rev. A **7**, 292 (1973).
[60] P. M. Mul, J. Wm McGowan, P. Defrance, and J. B. A. Mitchell, J. Phys. B **16**, 3099 (1983).
[61] N. G. Adams, D. Smith, and E. Alge, J. Chem. Phys. **81**, 1778 (1984).
[62] D. Smith and P. Spanel, Int. J. Mass Spectrom. Ion Processes **129**, 163 (1993).
[63] G. A. Raiche, J. B. Jeffries, K. J. Rensberger, and D. R. Crosley, J. Chem. Phys. **92**, 7258 (1990).
[64] G. H. Dieke and H. M. Crosswhite, J. Quantum Spectrosc. Radiat. Transfer **2**, 97 (1962).
[65] D. R. Crosley and R. K. Lengel, J. Quantum Spectrosc. Radiat. Transfer **15**, 579 (1975).
[66] K. Schofield, J. Phys. Chem. Ref. Data **8**, 723 (1979).
[67] M. F. Golde (unpublished).
[68] J. J. Margitan, F. Kaufman, and J. G. Anderson, Int. J. Chem. Kinet. Symp. No. 1, 281 (1975).
[69] D. Talbi and R. P. Saxon, J. Chem. Phys. **91**, 2376 (1989).
[70] D. R. Bates, Mon. Not. R. Astron. Soc. **263**, 369 (1993).
[71] L. H. Anderson, O. Heber, D. Kella, H. B. Petersen, L. Vejby-Christensen, and D. Zaifman, Phys. Rev. Lett. **77**, 4891 (1966).
[72] T. L. Williams, N. G. Adams, L. M. Babcock, Charles R. Herd, and M. Geoghegan, Mon. Not. R. Astron. Soc. **282**, 413 (1966).